



Article

# Antibacterial Properties of Rose Bengal Conjugated to Hyaluronic Acid

Melad Atrash, Iryna Hovor, Yanna Gurianov , Margarita Barel, Olga Semenova, Tamara Brider, Marina Nisnevitch and Faina Nakonechny \*

Department of Chemical Engineering, Ariel University, Kiryat-ha-Mada, Ariel 4070000, Israel

\* Correspondence: fainan@ariel.ac.il; Tel.: +972-39765786

**Abstract:** Dental diseases, including conditions affecting oral structures, have become more common due to unhealthy lifestyle choices. Traditional antibiotic treatments face challenges related to the development of antibiotic resistance in bacteria. Photodynamic antibacterial chemotherapy is emerging as a promising alternative using photosensitizers to generate reactive oxygen species upon exposure to light. This article examines the photosensitizer Rose Bengal (RB) immobilized in hyaluronic acid (HA) for prolonged antibacterial action. The RB-HA conjugate demonstrated a molar ratio of approximately three RB residues to each of the ten units of HA. RB-HA exhibited a high singlet oxygen quantum yield ( $\Delta\Phi = 0.90$ ), suggesting its efficacy in photodynamic treatment. A photostability analysis revealed slower photobleaching of RB-HA, which is essential for prolonged application. Under visible light and ultrasonic treatment, RB-HA exhibited effective antibacterial activity against Gram-positive *S. aureus* and Gram-negative *E. coli* bacteria for at least 80 days. The gradual release of RB ensured sustained bactericidal concentration. The study establishes RB-HA as a promising candidate for antimicrobial photodynamic and sonodynamic therapy in dental and other medical fields, providing enhanced stability and prolonged antibacterial efficacy.

**Keywords:** rose bengal; hyaluronic acid; conjugation; *S. aureus*; *E. coli*; photodynamic antibacterial activity; sonodynamic antibacterial activity; slow drug release



**Citation:** Atrash, M.; Hovor, I.; Gurianov, Y.; Barel, M.; Semenova, O.; Brider, T.; Nisnevitch, M.; Nakonechny, F. Antibacterial Properties of Rose Bengal Conjugated to Hyaluronic Acid. *Int. J. Mol. Sci.* **2024**, *25*, 3330. <https://doi.org/10.3390/ijms25063330>

Academic Editors: Silvana Alfei and Laura Mayol

Received: 26 January 2024

Revised: 4 March 2024

Accepted: 13 March 2024

Published: 15 March 2024



**Copyright:** © 2024 by the authors. Licensee MDPI, Basel, Switzerland. This article is an open access article distributed under the terms and conditions of the Creative Commons Attribution (CC BY) license (<https://creativecommons.org/licenses/by/4.0/>).

## 1. Introduction

Dental diseases, also known as oral diseases, encompass conditions that affect the teeth, gums, and other oral structures. Unhealthy lifestyle choices, such as unhealthy diets, processed foods, poor oral hygiene, and chronic stress, have contributed to the increased prevalence of these diseases [1–4]. As a consequence of these lifestyle choices, a significant portion of the population suffers from different dental problems, including periodontal diseases (gum diseases), and oral infections [5]. Without antibacterial treatment, these may cause damage to the supporting system of the tooth, including gum recession and bone loss in the jaw [6,7]. In many cases, the treatment of these bacteria is accomplished using antibiotics. However, the growth and spread of antibiotic-resistant bacteria can pose problems in the treatment of oral and dental diseases. Therefore, there is a need to search for new approaches to mitigate pathogenic bacteria [8–10].

Photodynamic Antibacterial Chemotherapy (PACT) presents promising prospects as an alternative to antibiotic treatment [11]. This therapy is performed using photosensitizers (PSs), which generate reactive oxygen species (ROS) under light [12]. This antimicrobial approach has a multi-targeted nature, making resistance development by bacteria unlikely. ROS in microbial cells damage various targets non-specifically, including nucleic acids, membrane-bound protein complexes, cytosolic enzymes, plasma membranes, and lipids. It is also supposed that PSs do not need to enter microbial cells, as adhesion to cell walls and membranes is enough for bacterial killing, bypassing resistance development [13]. PACT has become an essential tool in the field of dentistry, being used in a wide range

of specialized areas such as general dentistry, periodontics, orthodontics, endodontics, surgery, and implantology [14–16]. An additional method of the activation of PSs in the treatment of diseases of the oral cavity can be ultrasound. By combining ultrasound with photosensitizing agents, it is possible to enhance therapeutic outcomes [17]. Ultrasound can efficiently penetrate oral tissues, reaching areas that are difficult to access using conventional light sources. Ultrasound also activates PSs, leading to the production of ROS, which are responsible for the destruction of targeted oral pathogens. The use of PSs has advantages, such as reducing overall treatment time, eliminating the need for patient sedation, destroying bacterial cells, and combating multiresistant pathogens [18]. Additionally, PSs can be used in conjunction with other dental procedures, providing a non-invasive and versatile treatment option for a wide range of oral diseases [19]. However, saliva can dilute active ingredients in the mouth, biofilms reduce drug effects on microorganisms, and delivering drugs to specific sites such as the periodontal pocket is challenging. Therefore, carrier systems are required to consistently release them for effective concentrations. Advanced biomaterials like hydrogels, films, and nanoparticles hold promise as carriers for local drug delivery. These delivery systems offer advantages such as increasing drug solubility, prolonging action time, and reducing cytotoxicity [20,21].

Rose Bengal (RB) is a well-known PS that has strong antibacterial effects, which are not limited to a specific bacterial strain [22–24]. The probable bactericidal mechanism of RB involves the penetration of RB through bacterial cell walls and its binding to cell membranes, followed by the generation of reactive oxygen species under illumination conditions [25]. The high photodynamic activity of RB has been demonstrated against a variety of Gram-positive and Gram-negative bacteria, as well as against biofilms [25–27]. However, for medical use, it should be used in combination with materials that inhibit its rapid elimination from the body, allow it to concentrate exclusively in areas of inflammation, and exhibit a repeated effect.

The literature describes various approaches in which RB was combined with both organic and inorganic materials. In our previous works, we reported on RB immobilized in polymers to enable their reusability or continuous use. For instance, RB immobilized in low-density polyethylene through co-extrusion kept its photodynamic antibacterial activity for at least five days, and in polypropylene—for 11 days [28]. RB immobilized in polystyrene films effectively destroyed *S. aureus* and *E. coli* under illumination by white light for a week [29], and wastewater bacteria—for a month [30]. In addition, organically modified silica matrices with incorporated RB illuminated with white light kept high activity against bacteria for more than 10 cycles of use [31].

RB also exhibited photodynamic antibacterial properties when bound to a tissue-mimetic collagen matrix [32], chitosan [33], and furfuryl-modified gelatin [34]. However, in these studies, the reusability or continuous use of RB has not been examined.

Based on the literature data, we chose hyaluronic acid (HA) as a matrix for conjugation with RB and obtaining a long-term PS for the treatment of oral infections. HA has multiple medical applications due to high hygroscopicity and good biocompatibility when the half-life of HA in humans is weeks [35]. We assumed that the conjugation of RB with an HA matrix would possibly gradually release RB over an extended period, maintaining an RB concentration sufficient for antibacterial activity specifically in the target area, thus minimizing potential side effects.

The aim of the present work was to study the in vitro effects of the conjugate RB-HA against Gram-positive (*S. aureus*) and Gram-negative (*E. coli*) bacteria under white light illumination and ultrasonic treatment.

## 2. Results and Discussion

### 2.1. Characterization of RB-HA Conjugate

#### 2.1.1. Composition of RB-HA Conjugate

To determine the composition of the conjugate, the latter was dissolved in NaOH solution, and the RB concentration was measured using a calibration curve of free RB

dissolved in NaOH of the same concentration. Then, the content of RB in the conjugate and the molar ratio of RB to HA in the conjugate was calculated, which was 0.31, i.e., approximately three RB residues are bonded to each ten units of HA.

### 2.1.2. FTIR Assay of RB-HA

The HA structure includes carboxyl and hydroxyl functional groups and ether and amide bonds (Figure 1a), which are reflected in the FTIR spectrum of HA (Figure 2) with bands at  $3282\text{ cm}^{-1}$  (a broad band of OH and NH stretching),  $2859\text{ cm}^{-1}$  (NH stretching),  $1601\text{ cm}^{-1}$  (NH bending) [36],  $1539\text{ cm}^{-1}$  and  $1402\text{ cm}^{-1}$  (antisymmetric and symmetric stretching of the amide group, respectively) [37],  $1375\text{ cm}^{-1}$  and  $1355\text{ cm}^{-1}$  (OH bending in carboxyl and hydroxyl groups, respectively),  $1126\text{ cm}^{-1}$  (ester CO stretching) [36], and  $1025\text{ cm}^{-1}$  (the vibrational modes of  $-\text{CH}_2\text{OH}$  groups of carbohydrates) [38]. The FTIR spectrum of RB contains bands corresponding to its structure (Figures 1b and 2):  $3360\text{ cm}^{-1}$  and  $2969\text{ cm}^{-1}$  (OH stretching) [36],  $1609\text{ cm}^{-1}$  (CH bending in the aromatic ring) [36],  $1232\text{ cm}^{-1}$  and  $1127\text{ cm}^{-1}$  (CO stretching) [36],  $1439\text{ cm}^{-1}$  (aromatic ring C–C stretching) [39],  $1412\text{ cm}^{-1}$  and  $950\text{ cm}^{-1}$  (OH bending) [36],  $757\text{ cm}^{-1}$ ,  $657\text{ cm}^{-1}$  and  $610\text{ cm}^{-1}$  (C–Cl stretching), and  $566\text{ cm}^{-1}$  and  $516\text{ cm}^{-1}$  (C–I stretching) [36]. Two bands,  $1540$  and  $1490\text{ cm}^{-1}$ , are assigned to asymmetrical and symmetrical stretching vibrations of  $\text{COO}^-$ , respectively [40]. Actually, carboxylates are characterized by two intense bands in the ranges of  $1650\text{--}1540\text{ cm}^{-1}$  and  $1450\text{--}1360\text{ cm}^{-1}$ , and the  $1540\text{ cm}^{-1}$  signal in the RB spectrum can be definitely related to the carboxylate group, but although the  $1490\text{ cm}^{-1}$  band seems to lie outside the  $1450\text{--}1360\text{ cm}^{-1}$  range, we still assign it to  $\text{COO}^-$ , explaining this shift through dipole–dipole interactions [41,42]. In the spectrum of the RB-HA conjugate (Figure 2), the bands at  $1375\text{ cm}^{-1}$  and  $1490\text{ cm}^{-1}$  assigned to OH bending in carboxyl groups and symmetrical stretching vibrations of  $\text{COO}^-$ , respectively, are absent. These changes prove the involvement of these groups in the formation of new bonds in the RB-HA conjugate. In addition, a band at  $1025\text{ cm}^{-1}$ , typical for the  $-\text{CH}_2\text{OH}$  groups of carbohydrates and is thus absent in the spectrum of RB, appears in the spectrum of the conjugate along with bands characteristic for RB groups. Since RB and HA are connected through diaminopropane, providing amide bonds, which are already present in the HA structure (Figure 1a), the appearances of new amide bonds cannot be registered in the FTIR spectrum of the conjugate. The bands  $2359\text{ cm}^{-1}$  and  $2334\text{ cm}^{-1}$ , which are present in all the spectra, are due to characteristic vibrations of  $\text{CO}_2$  in the air [36].

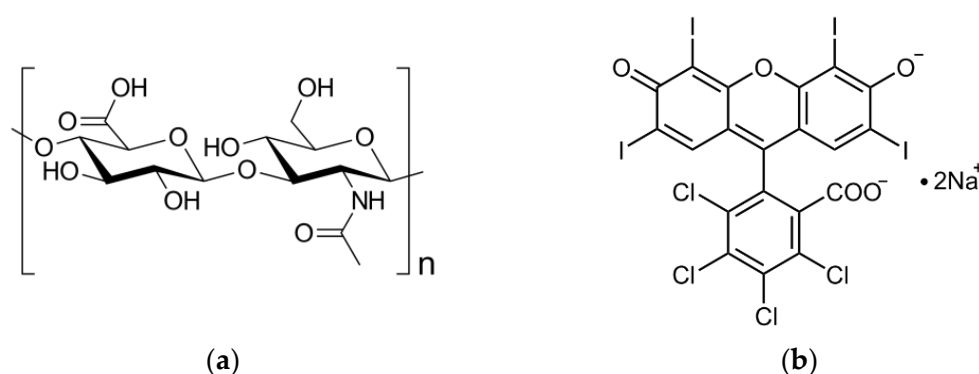


**Figure 1.** The structural formulas of hyaluronic acid (HA) (a) and Rose Bengal (RB) (b).

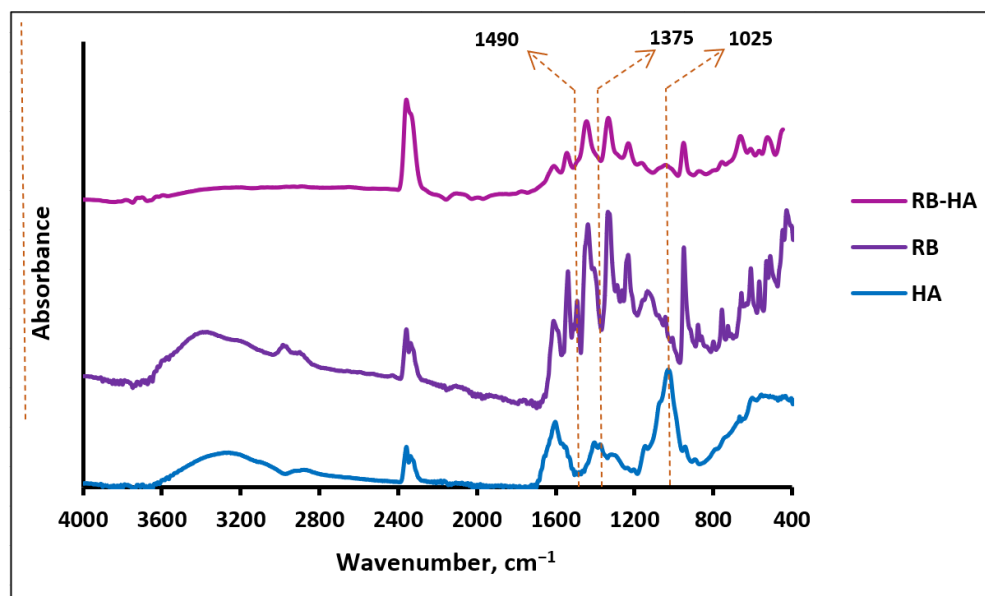


**Figure 2.** The FTIR spectra of HA, RB, and RB-HA.

## 2.2. Generation ROS by RB-HA

The formation of ROS is the most significant property of PSs. The singlet oxygen quantum yield ( $\Delta\Phi$ ), or the amount of singlet oxygen produced, characterizes the abilities of molecules to be PSs in PDT applications [18]. It is known that RB generates free oxygen radicals when exposed to light [22,43]. However, it was necessary to test whether the RB-HA conjugate was capable of producing ROS as well. Absorption spectra of RB and RB-HA in saline were measured and compared to the emission spectrum of the white LED lamp used in this study (Figure 3). It can be seen that the absorption spectra of the compounds fully overlap with the emission spectrum of the LED lamp, and therefore, this light source can be applied in photodynamic studies.

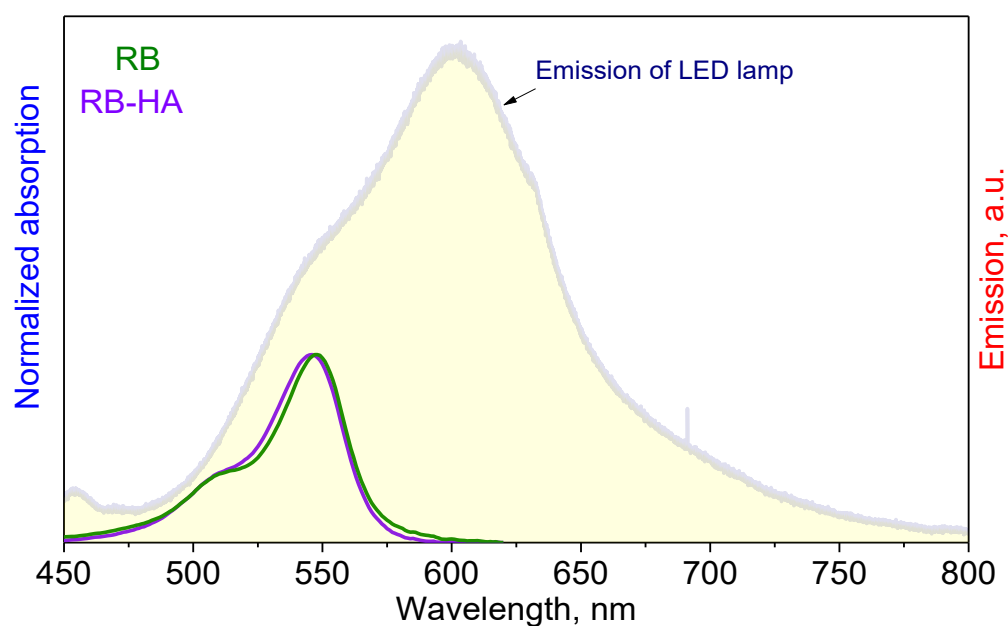


**Figure 3.** The spectral overlap between the absorption spectra of the RB and RB-HA in saline and the emission spectrum of the LED lamp.

The singlet oxygen generation by RB-HA under the LED lamp was measured in methanol using DPBF and compared to the ROS generation by RB (Figure 4). DPBF is a fluorescent probe that reacts with some ROS, resulting in the formation of endoperoxides, which leads to the decomposition of the probe [44–46]. This process can be monitored spectrophotometrically since this process is accompanied by a decrease in the absorption of DPBF at 410 nm. Figure 4a shows that the absorption of DPBF alone did not change in time. However, the absorption of DPBF drops drastically when irradiated in the presence of RB and RB-HA (Figure 4b,c). The decrease in the absorption in time enabled us to calculate the DPBF degradation rate constant  $k$  (Figure 4d) [47,48]. The degradation rate constants for RB and RB-HA were  $0.063 \text{ min}^{-1}$  and  $0.071 \text{ min}^{-1}$ , respectively. The difference between these values was not statistically significant ( $p$ -value = 0.68), suggesting that the ROS generation by RB is not substantially altered when it is conjugated.

The obtained constants allowed for the determination of the singlet oxygen quantum yield ( $\Delta\Phi$ ) of RB-HA, using the following equation [49,50]:

$$\Delta\Phi_{\text{RB-HA}} = \Delta\Phi_{\text{RB}} \times k_{\text{RB-HA}}/k_{\text{RB}}$$

The singlet oxygen quantum yield of RB was reported to be  $\Delta\Phi = 0.80$  in methanol [51], and that calculated for RB-HA was  $\Delta\Phi = 0.90$ . Thus, the conjugate demonstrated a higher rate of singlet oxygen production than the free RB, which shows the potential of this compound as a PS in PDT applications.

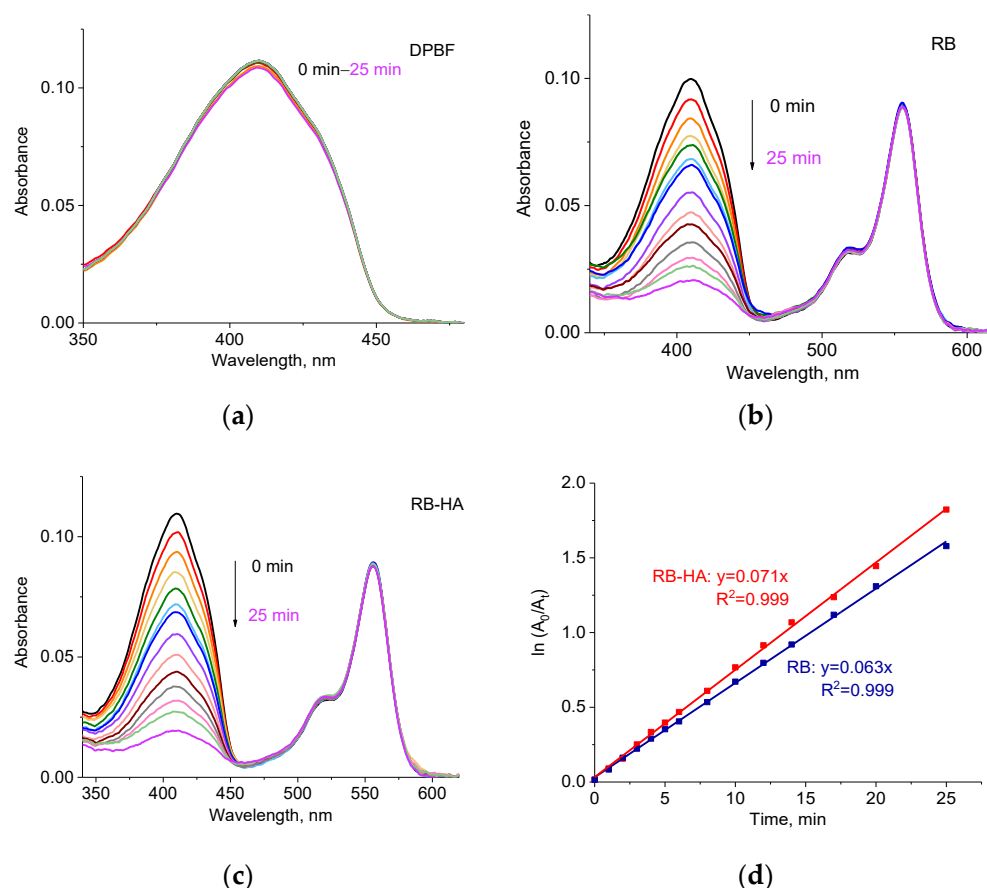


**Figure 4.** (a) Absorption spectra of DPBF under LED lamp irradiation; absorption spectra of RB (b) and RB-HA (c) with DPBF under LED lamp irradiation; time-dependent decomposition of DPBF through singlet oxygen produced by RB and RB-HA (d).

Interestingly, ROS formation was not observed under ultrasonic treatment. The behavior of DPBF in the presence of RB or RB-HA did not differ from that of DPBF alone.

### 2.3. Photostability of RB-HA Conjugate

The important factor in PDT is the photostability of the PS since a high rate of photodegradation under illumination may lead to insufficient ROS production and make the PS not applicable for effective PDT. The photostability of PSs can be monitored through changes in the absorption spectra, during light irradiation.

RB is known to be photostable since its half-life time, or the time it takes the concentration of a reactant to reach half of its initial value, reaches values of tens of minutes [52,53]. The photostability of the RB-HA conjugate was compared to that of free RB and tested under the experimental conditions used for illumination in photodynamic experiments. The initial optical densities of RB and RB-HA were equal.

Figure 5 shows decreases in the absorption spectra of RB (a) and RB-HA (b) under irradiation by LED lamp. The drop in normalized absorbance at 547 nm in time was less considerable in the case of conjugated RB than for the free one (Figure 5c). The absorption decay half-lives were calculated from the obtained monoexponential decay functions and were 48 min and 104 min for RB and RB-HA, respectively. The calculated kinetic constants of decomposition rate ( $k$ ), determined as a slope of the  $\ln(A_0/A_t)$  vs. time plot (Figure 5d) [54], were  $k = 0.01201 \text{ min}^{-1}$  for RB and  $k = 0.00385 \text{ min}^{-1}$  for RB-HA, which indicated that the process of the photodegradation of RB-HA was three times slower than of RB. This difference was proven statistically with a  $p$ -value of 0.0014. We consider that RB-HA exhibits higher photostability than RB, which is crucial for PDT applications.

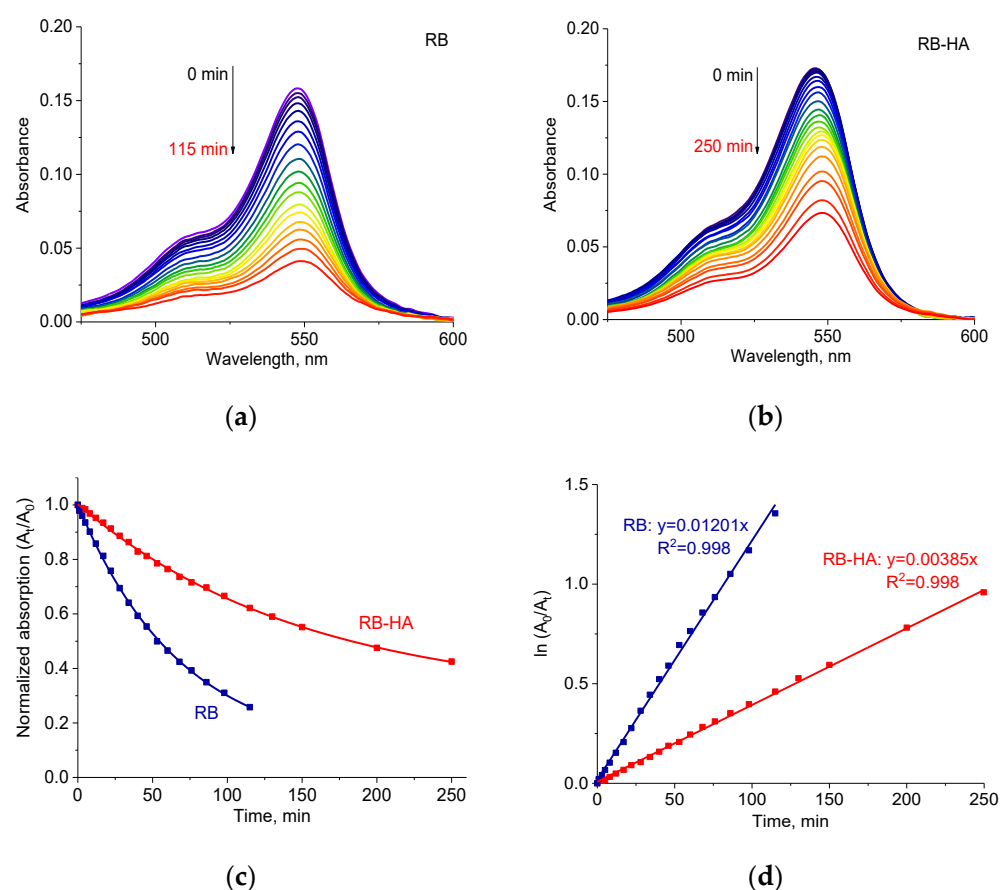


**Figure 5.** Absorption spectra of RB (a) and RB-HA (b) under light irradiation by LED lamp and time-dependent decomposition of RB and RB-HA (c,d).  $A_0$  and  $A_t$  are absorption values at zero and illumination time periods.

### 2.4. Photo- and Sonodynamic Activity of RB-HA

First of all, the dark toxicity of RB-HA was examined, as high concentrations of free RB are known to reduce cell viability without irradiation, a phenomenon referred to as

dark antibacterial toxicity [55,56]. In this case, the inhibition of bacterial growth occurs in a manner distinct from the photodynamic mechanism, when the photooxidation of PSs involves the excitation of triplet oxygen, leading to the production of cytotoxic reactive oxygen species. Actually, the mechanism of dark toxicity is still being investigated [25]. To study the dark antibacterial activity of RB-HA, cells of *S. aureus* and *E. coli* were incubated in the dark in the presence of free or conjugated RB at various concentrations, and then, the cell viability was tested (Figure 6). At the same time, the antibacterial activity of free RB was tested under light and ultrasound irradiation (Figure 6).

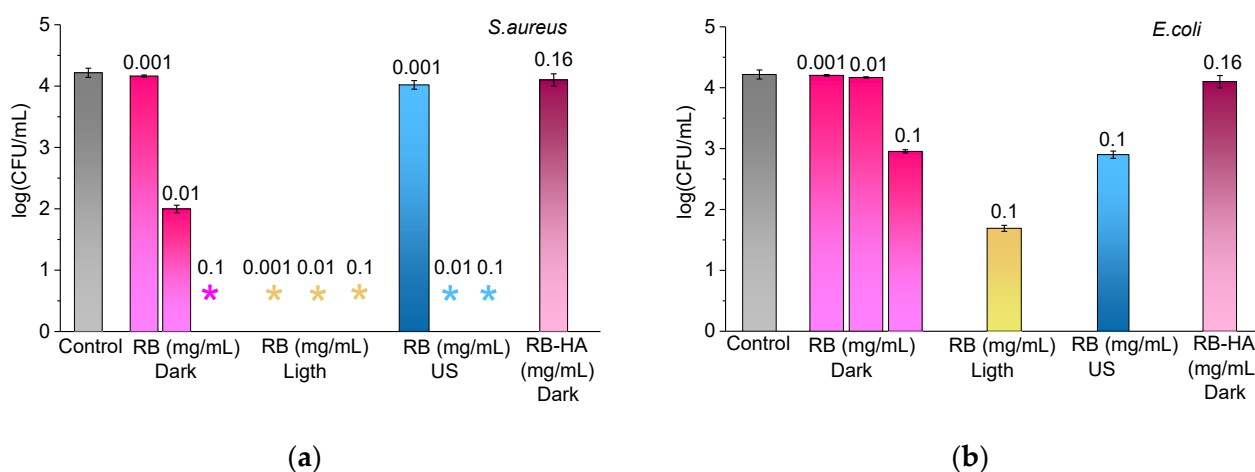


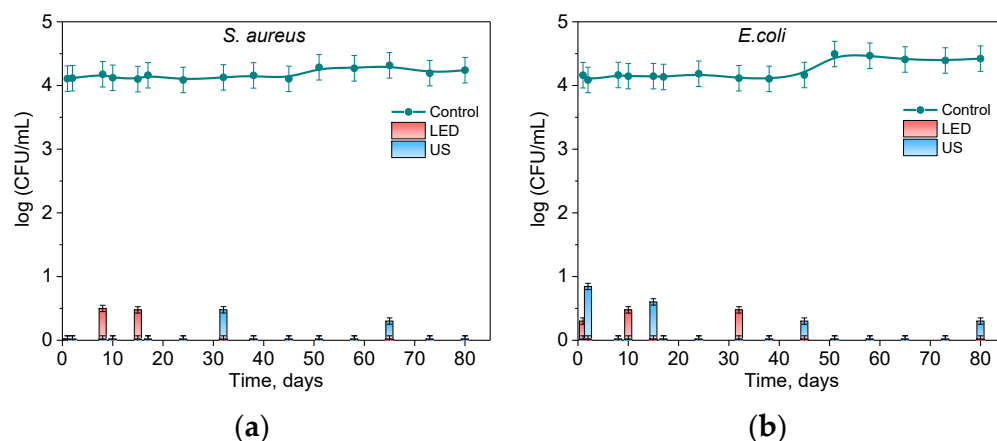
**Figure 6.** The effects of RB and RB-HA at different concentrations in the inactivation of *S. aureus* (a) and *E. coli* (b) cells at concentrations of  $10^4$  CFU/mL in the dark, under illumination and ultrasonic treatment. The asterisk \* indicates the total inhibition of bacterial cells.

The experiment showed that in the dark, *S. aureus* was eradicated at an RB concentration of 0.1 mg/mL, whereas at 0.01 mg/mL, the cells were only partially inactivated, and at 0.001 mg/mL, remained intact (Figure 6a). Moreover, at all three RB concentrations, *S. aureus* was eradicated under exposure to white light. When treated using ultrasound, bacteria survived only at the lowest RB concentration of 0.001 mg/mL. Another situation was seen in the case of *E. coli*, when, only at 0.1 mg/mL RB, the cell concentration decreased by 1 log<sub>10</sub> (Figure 6b), and RB at 0.001 and 0.01 mg/mL did not affect the viability of *E. coli*. Under illumination and ultrasonic irradiation in the presence of 0.1 mg/mL RB, the count of alive cells was lower than at dark conditions, but the complete eradication of *E. coli* cells was not reached. The results obtained for both bacteria were compared to a slightly higher concentration of RB-HA 0.16 mg/mL. As can be seen in Figure 6, at this concentration of the conjugate, the bacteria completely survived. Thus, this concentration was used for subsequent experiments.

The bacterial survival was also examined under LED light and sonication in the absence of RB and RB-HA. Cells of *S. aureus* treated for 10 min, and of *E. coli*, for 20 min, remained intact and served as a control in each case. The treatments during 10 min for *S. aureus* and 20 min for *E. coli* had no impact on viability.

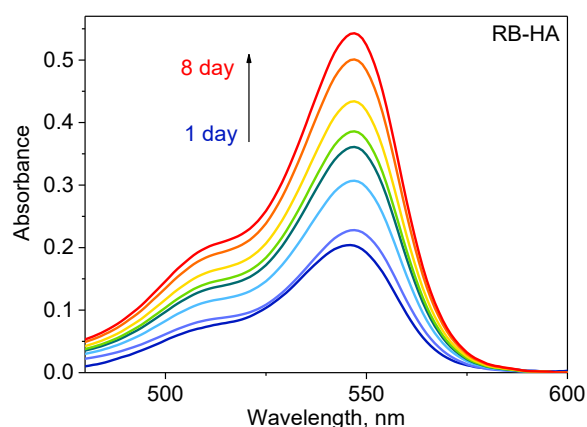
To estimate the antibacterial activity of RB-HA, equal portions of the conjugate were distributed into a number of glass transparent vials. Once or twice a week, cells of Gram-positive *S. aureus* and Gram-negative *E. coli* bacteria were added to the vials, either illuminated or sonicated, and then tested for viability.

Figure 7 demonstrates the antibacterial activity of the RB-HA conjugate against *S. aureus* (Figure 7a) and *E. coli* (Figure 7b) upon illumination with visible light and ultrasonic treatment. It can be seen that RB-HA was effective in killing both types of microorganisms and kept its activity under repeated use for at least 80 days. In all cases, the bacteria were either totally killed or strongly inhibited when their concentration dropped by ca. 3.5 log<sub>10</sub>.



**Figure 7.** Inhibition of *S. aureus* (a) and *E. coli* (b) by RB-HA under illumination (LED) and sonication (US). Control — cells, illuminated or sonicated in the absence of RB-HA.

We assumed that the continuous gradual release of RB from the conjugate provided a long-term bactericidal concentration of PS in the medium. To examine this possibility, the solution of RB-HA in saline was incubated for 8 days in the dark and monitored using a measurement of absorbance (Figure 8).



**Figure 8.** UV spectra of RB-HA in saline kept in the dark at an ambient temperature.

As can be seen from Figure 8, during the experiment, the absorption increased in time. The obtained result demonstrated a gradual release of RB from the conjugate. This observation is also confirmed by changes in the RB concentration in the solutions used in the experiments for testing antibacterial activity. In the experiment on testing the antibacterial activity of RB-HA, on day 80, the concentration of free RB in the vials that underwent illumination was 0.018 mg/mL, and in those that were treated with ultrasound — 0.23 mg/mL. Thus, the long-term antibacterial effect of RB-HA under illumination is explained by the high ability of the conjugate to produce a high rate of ROS when the concentration of released RB was definitely not sufficient for the dark activity of RB. In the case of ultrasound treatment, we showed that RB did not generate ROS under our experimental conditions. However, the sonication of the conjugate led to a significant increase in the concentration of free RB up to that of dark toxicity. In addition, ultrasonic treatment is known to improve cell sensitivity to RB [29,57]. These factors led to the complete killing of bacteria.

### 3. Methods and Materials

#### 3.1. Synthesis and Characterization of RB-HA Conjugate

All the chemicals used in this study were of analytical grade: hyaluronic acid (HA)—MW 30–50 kDA, Glentham Life Sciences Ltd., Corsham, England; 1,2-Diaminopropane, 99%

(PDA)—Thermo Fisher Scientific, Fair Lawn, NJ, USA; carbodiimide [N-ethyl-N = -(3-dimethylaminopropyl) carbodiimide (EDC)—Glenthams Life Sciences Ltd., Corsham, England; hydroxybenzotriazole (HOBt)—Sigma-Aldrich Chemie GmbH, Steinheim, Germany; and Rose Bengal (RB)—Alfa Aesar, Heysham, England.

The conjugate RB-HA was synthesized using chemical cross-linking via EDC using a PDA linker. The solution of HA (0.1 g) was prepared in 30 mL of distilled water and stirred in a shaker until the HA dissolved. Then, 0.4 mL of PDA was added to the HA solution and stirred using the vortex. EDC (1.15 g, 6 mM) and HOBt (0.81 g, 6 mM) were dissolved in a 20 mL mixture of DMSO–distilled water (1:1). The obtained solutions were mixed in a flask and stirred overnight at 120 rpm. After that, 20 mL of a solution containing RB (1 g, 51.4 mM), EDC (1.15 g, 6 mM), and HOBt (0.81 g, 6 mM) in a mixture of DMSO–distilled water (1:1) were added, and the solution was further stirred in the dark. The conjugated product was then dialyzed against distilled water using a dialysis membrane (cellulose tubing; Sigma-Merck, Darmstadt, Germany) for one week and then lyophilized. The obtained conjugate RB-HA was stored at  $-20\text{ }^{\circ}\text{C}$  in dark tubes.

### 3.2. Checking the RB Load in the Conjugate

To assess the RB load in the conjugate, an accurately weighed amount of 10 mg of the conjugate was dissolved in 10 mL of 1 M NaOH solution, and its absorbance was measured at 548 nm using a spectrophotometer (Evolution 201; Thermo Fisher Scientific Inc., Madison, WI, USA), and the RB concentration was calculated using a calibration curve. It enabled us to calculate the amount of the released RB and to calculate the mass and molar ratio between the RB and HA.

### 3.3. FTIR Analysis

The samples were analyzed using an FTIR spectrometer (Jasco, 6800 FV, Tokyo, Japan) at room temperature in the  $4000\text{--}400\text{ cm}^{-1}$  range at an operation number of 64 scans, a resolution of  $2.0\text{ cm}^{-1}$ , and a scanning interval of  $1\text{ cm}^{-1}$ . The spectra were analyzed using Spectra Analysis™ (Jasco, Tokyo, Japan).

### 3.4. Spectral Studies and Photostability Tests

The emission spectrum of the white LED lamp used for illumination was registered using the HORIBA spectrometer (Jobin Yvon Inc., Edison, NJ, USA) equipped with a monochromator FHR1000 and detector CCD (HORIBA Scientific's Synapse™, Irvine, CA, USA).

Photostability was measured in saline in 1 cm quartz cuvettes at RT during irradiation with the LED lamp. Absorption spectra were recorded before light treatment and during irradiation using a Thermo Scientific Evolution 201 spectrophotometer. The initial absorbance values of the RB and RB-HA at the absorption maximum were  $\sim 0.16$ . The ratios ( $A_t/A_0$ ) and  $\ln(A_0/A_t)$  of the measured absorbencies at the long-wavelength maximum before ( $A_0$ ) and after exposure ( $A_t$ ) were used to plot decay curves. The photostability experiment for each sample was performed 3 times and the average decay curve was obtained.

### 3.5. Generation of ROS

The singlet oxygen generation (ROS) of RB-HA was measured in methanol with 1,3-diphenylisobenzofuran (DPBF) as the singlet oxygen scavenger, following the procedure in [58]. RB was used as the reference dye. The initial absorbance values of the RB and RB-HA at 555 nm were  $\sim 0.09$ . Samples were light-irradiated in a standard 1 cm quartz cuvette using the LED lamp. The corresponding plot  $\ln(A_0/A_t)$  vs. time, representing the absorbance of DPBF at 410 nm at zero ( $A_0$ ) and during irradiation ( $A_t$ ), was drawn and fitted using a first-order reaction rate function.

### 3.6. Bacterial Growth

Cultures of Gram-positive bacteria *S. aureus* (ATCC 25923) and Gram-negative bacteria *E. coli* (ATCC 25922) were grown on Brain Heart agar plates (BHA, Acumedia, Lansing, MI, USA) for 24 h, transferred into Brain Heart broth (BH, Acumedia, Lansing, MI, USA), grown at  $37 \pm 1$  °C with shaking at 170 rpm until reaching the absorbance of  $OD_{660} \approx 0.3$ , and diluted with commercially available sterile 0.9% saline solution to  $OD_{660} = 0.10 \pm 0.02$ , which corresponds to a cell concentration of  $10^8$  CFU mL<sup>-1</sup>. Then, the cells were diluted using saline to the final concentration of  $10^5$  CFU mL<sup>-1</sup>. The obtained cell suspension was used for further experiments.

### 3.7. Antimicrobial Activity Test

The dark toxicity of RB-HA was examined in a comparison to different concentrations of RB. The 3 mL of suspensions containing cells  $10^4$  CFU mL<sup>-1</sup> with RB in concentrations of 0.1, 0.01, and 0.001 mg/mL and RB-HA in a concentration of 0.16 mg/mL were prepared. Then, the solutions were kept in a shaker at 100 rpm and in the dark for 10 and 20 min for *S. aureus* and *E. coli*, respectively. Then, 0.1 mL of the solutions were cultured on BH agar plates overnight at  $37 \pm 1$  °C in the dark. The bacterial colony-forming units (CFU) were counted using a Scan 500 colony counter (Interscience, Saint-Nom-la Bretèche, France).

An antimicrobial activity test of the RB-HA conjugate was carried out in glass vials with lids for 80 days. The RB-HA (50 mg) was dissolved in saline (2.7 mL), and this volume was monitored during the test. The suspensions of the cells  $10^5$  CFU mL<sup>-1</sup> (0.3 mL) were added to the RB-HA solution before each experiment. Thus, the study was conducted under the same conditions at a cell concentration of  $10^4$  CFU mL<sup>-1</sup> in 3 mL of the mixture. During exposure to light or ultrasound for certain periods of time, 0.1 mL was taken from the samples and cultured on BH agar plates overnight at  $37 \pm 1$  °C in the dark, and then the CFUs were counted. Between the experiments, the bottles with RB-HA were kept in the dark in an incubator at 25 °C.

Light irradiation was carried out using a 18 W LED lamp (ORSAM, model L18W/765, cool daylight, Munich, Germany), under shaking at 100 rpm. The lamp, which emitted light between 400 and 800 nm with a fluence rate of  $7.1$  mW cm<sup>-2</sup> and light intensity of 35 klux, was used for all experiments. Light intensity was measured using an LX-102 light meter (Lutron, Taipei, Taiwan). The samples were placed in front of a lamp at a distance of 20 cm, and doses were  $4$  J cm<sup>-2</sup> and  $8$  J cm<sup>-2</sup> for *S. aureus* and *E. coli*, respectively.

Ultrasound exposure was carried out in an ultrasonic bath VUO3H (SMEG Instruments, Guastalla, Italy) at a frequency of 38 kHz. The sampling time was similar to that in the light irradiation experiment.

### 3.8. Statistical Analysis

The results obtained from at least three independent experiments carried out in duplicates were analyzed through single-factor ANOVA analyses. The differences between the results were considered significant when the *p*-value was less than 0.05. Quantitative results are presented as the mean  $\pm$  standard error.

## 4. Conclusions

This paper presents a comprehensive analysis of the RB-HA conjugate we synthesized, providing insight into its composition, structure, singlet oxygen generation, photostability, and photo- and sonodynamic activity. The RB-HA conjugate demonstrated the ability to generate ROS upon exposure to LED light, indicating the potential for applications of the conjugate as a PS in photodynamic therapy (PDT). The singlet oxygen quantum yield ( $\Delta\Phi$ ) of RB-HA under illumination with an LED lamp was close to the parameters of free RB. The RB-HA conjugate exhibited higher photostability and a slower photodegradation rate compared to free RB. The process of the photodegradation of RB-HA was three times slower than that of free RB. RB-HA demonstrated antibacterial activity against Gram-positive (*S. aureus*) and Gram-negative (*E. coli*) bacteria under visible light illumination and ultrasoni-

cation. Bacteria were either totally killed or strongly inhibited. The gradual release of RB from the conjugate ensured a constant and sufficient bactericidal concentration of PS in the medium over a long period (at least 80 days), wherein the conjugate did not exhibit dark toxicity towards bacterial cells. Thus, the RB-HA conjugate shows good prospects for use as an antibacterial agent with efficient singlet oxygen generation, improved photostability, and sustained antibacterial activity, making it a potential candidate for use in antimicrobial photodynamic and sonodynamic therapy in dental and other diseases.

**Author Contributions:** Conceptualization, F.N. and M.N.; methodology, F.N., I.H. and O.S.; investigation, M.A., M.B., Y.G., O.S., T.B. and I.H.; resources, M.N.; data curation, F.N.; writing—original draft preparation, M.A.; writing—review and editing, I.H., M.N. and F.N.; supervision, M.N. and F.N.; project administration, F.N. All authors have read and agreed to the published version of the manuscript.

**Funding:** This research received no external funding.

**Institutional Review Board Statement:** Not applicable.

**Informed Consent Statement:** Not applicable.

**Data Availability Statement:** The data are available in the current publication.

**Acknowledgments:** We acknowledge the Research Authority of Ariel University, Israel, for supporting this research. We are very grateful to B.Sc. students Noy Yaish, Einav Musli, Lital Moshe, Shahar Dvide, Gehad Albaba, Noa Shamir, and Noa Fridman. We want to thank Michael Shuldiner and Shmuel Sternklar for their kind help with the measurement of LED emissions.

**Conflicts of Interest:** The authors declare no conflicts of interest.

## References

- Baelum, V. Dentistry and Population Approaches for Preventing Dental Diseases. *J. Dent.* **2011**, *39*, S9–S19. [[CrossRef](#)]
- Peres, M.A.; Macpherson, L.M.D.; Weyant, R.J.; Daly, B.; Venturelli, R.; Mathur, M.R.; Listl, S.; Celeste, R.K.; Guarnizo-Herreño, C.C.; Kearns, C.; et al. Oral Diseases: A Global Public Health Challenge. *Lancet* **2019**, *394*, 249–260. [[CrossRef](#)]
- Kane, S.F. The Effects of Oral Health on Systemic Health. *Gen. Dent.* **2017**, *65*, 30–34.
- Laudenbach, J.M.; Kumar, S.S. Common Dental and Periodontal Diseases. *Dermatol. Clin.* **2020**, *38*, 413–420. [[CrossRef](#)]
- El Kholi, K.; Genco, R.J.; Van Dyke, T.E. Oral Infections and Cardiovascular Disease. *Trends Endocrinol. Metab.* **2015**, *26*, 315–321. [[CrossRef](#)] [[PubMed](#)]
- Cardoso, E.M.; Reis, C.; Manzanares-Céspedes, M.C. Chronic Periodontitis, Inflammatory Cytokines, and Interrelationship with Other Chronic Diseases. *Postgrad. Med.* **2018**, *130*, 98–104. [[CrossRef](#)] [[PubMed](#)]
- Zheng, X.; He, J.; Wang, L.; Zhou, S.; Peng, X.; Huang, S.; Zheng, L.; Cheng, L.; Hao, Y.; Li, J.; et al. Ecological Effect of Arginine on Oral Microbiota. *Sci. Rep.* **2017**, *7*, 7206. [[CrossRef](#)] [[PubMed](#)]
- Ahmadi, H.; Ebrahimi, A.; Ahmadi, F. Antibiotic Therapy in Dentistry. *Int. J. Dent.* **2021**, *2021*, 6667624. [[CrossRef](#)]
- Plotniece, A.; Sobolev, A.; Supuran, C.T.; Carta, F.; Björkling, F.; Franzyk, H.; Yli-Kauhaluoma, J.; Augustyns, K.; Cos, P.; De Vooght, L.; et al. Selected Strategies to Fight Pathogenic Bacteria. *J. Enzyme Inhib. Med. Chem.* **2023**, *38*, 2155816. [[CrossRef](#)] [[PubMed](#)]
- Saravanan, A.; Das, P.; Maruthapandi, M.; Aryal, S.; Michaeli, S.; Mastai, Y.; Luong, J.H.T.; Gedanken, A. Heteroatom Co-Doping (N, NS, NB) on Carbon Dots and Their Antibacterial and Antioxidant Properties. *Surf. Interfaces* **2024**, *46*, 103857. [[CrossRef](#)]
- Mahmoudi, H.; Bahador, A.; Pourhajibagher, M.; Alikhani, M.Y. Antimicrobial Photodynamic Therapy: An Effective Alternative Approach to Control Bacterial Infections. *J. Lasers Med. Sci.* **2018**, *9*, 154–160. [[CrossRef](#)]
- Anas, A.; Sobhanan, J.; Sulfiya, K.M.; Jasmin, C.; Sreelakshmi, P.K.; Biju, V. Advances in Photodynamic Antimicrobial Chemotherapy. *J. Photochem. Photobiol. C Photochem. Rev.* **2021**, *49*, 100452. [[CrossRef](#)]
- Marasini, S.; Leanse, L.G.; Dai, T. Can Microorganisms Develop Resistance against Light Based Anti-Infective Agents? *Adv. Drug Deliv. Rev.* **2021**, *175*, 113822. [[CrossRef](#)]
- Takasaki, A.A.; Aoki, A.; Mizutani, K.; Schwarz, F.; Sculean, A.; Wang, C.Y.; Koshy, G.; Romanos, G.; Ishikawa, I.; Izumi, Y. Application of antimicrobial photodynamic therapy in periodontal and peri-implant diseases. *Periodontol. 2000* **2009**, *51*, 109–140. [[CrossRef](#)] [[PubMed](#)]
- Silva, T.; Lunardi, A.J.L.; Barros, A.C.S.M.; Mandetta, A.R.H.; Grudzien, E.; San-Martín, M.; Horliana, A.C.R.T.; Bussadori, S.K.; Motta, L.J. Application of Photodynamic Therapy in Pediatric Dentistry: Literature Review. *Pharmaceutics* **2023**, *15*, 2335. [[CrossRef](#)] [[PubMed](#)]
- Sachdeva, A. Photodynamic therapy in dentistry: A literature review. *J. Dent. Panacea* **2023**, *5*, 17–20. [[CrossRef](#)]

17. Roy, J.; Pandey, V.; Gupta, I.; Shekhar, H. Antibacterial Sonodynamic Therapy: Current Status and Future Perspectives. *ACS Biomater. Sci. Eng.* **2021**, *7*, 5326–5338. [[CrossRef](#)] [[PubMed](#)]
18. Correia, J.H.; Rodrigues, J.A.; Pimenta, S.; Dong, T.; Yang, Z. Photodynamic Therapy Review: Principles, Photosensitizers, Applications, and Future Directions. *Pharmaceutics* **2021**, *13*, 1332. [[CrossRef](#)]
19. Dharshana, S.; Krishnan, V.; Divya, V. Therapeutic Applications of Ultrasound in Dentistry. *J. Pharm. Sci. Res.* **2020**, *12*, 1394–1399.
20. Zhang, Y.; Jiang, R.; Lei, L.; Yang, Y.; Hu, T. Drug delivery systems for oral disease applications. *J. Appl. Oral. Sci.* **2022**, *30*, e20210349. [[CrossRef](#)]
21. Hosseinpour-Moghadam, R.; Mehryab, F.; Torshabi, M.; Haeri, A. Applications of Novel and Nanostructured Drug Delivery Systems for the Treatment of Oral Cavity Diseases. *Clin. Ther.* **2021**, *43*, e377–e402. [[CrossRef](#)]
22. Sabbahi, S.; Ben Ayed, L.; Jemli, M. Staphylococcus Aureus Photodynamic Inactivation Mechanisms by Rose Bengal: Use of Antioxidants and Spectroscopic Study. *Appl. Water Sci.* **2018**, *8*, 56. [[CrossRef](#)]
23. Niazi, F.H.; Qamar, Z.; Noushad, M.; Muhareb, A.K. Bin Use of Rose Bengal, Methylene Blue and Curcumin Photosensitizers Activated Using Light Emitting Diode on Post Space Disinfection Bonded to Fiber Post: An Assessment of Extrusion Bond Strength. *Pakistan J. Med. Sci.* **2022**, *38*, 34–39. [[CrossRef](#)]
24. Ghoniem, D.F.; Abdelkawi, S.A.; Fadel, M.; Abdel Fadeel, D.; Fouly, M.; El-Kholy, A.I.; Hassan, A.A. Novel Photodynamic/Photothermal Treatment of Fungal Keratitis Using Rose Bengal-Loaded Polypyrrole-Gold Nanoparticles in Wistar Albino Rats. *J. Ocul. Pharmacol. Ther.* **2023**, *39*, 379–388. [[CrossRef](#)]
25. Kurosu, M.; Mitachi, K.; Yang, J.; Pershing, E.V.; Horowitz, B.D.; Wachter, E.A.; Lacey, J.W.; Ji, Y.; Rodrigues, D.J. Antibacterial Activity of Pharmaceutical-Grade Rose Bengal: An Application of a Synthetic Dye in Antibacterial Therapies. *Molecules* **2022**, *27*, 322. [[CrossRef](#)]
26. Nisnevitch, M.; Nakonechny, F.; Nitzan, Y. Photodynamic Antimicrobial Chemotherapy by Liposome-Encapsulated Water-Soluble Photosensitizers. *Russ. J. Bioorg. Chem.* **2010**, *36*, 363–369. [[CrossRef](#)] [[PubMed](#)]
27. Silva, A.F.; Borges, A.; Freitas, C.F.; Hioka, N.; Mikcha, J.M.G.; Simões, M. Antimicrobial Photodynamic Inactivation Mediated by Rose Bengal and Erythrosine Is Effective in the Control of Food-Related Bacteria in Planktonic and Biofilm States. *Molecules* **2018**, *23*, 2288. [[CrossRef](#)] [[PubMed](#)]
28. Valkov, A.; Nakonechny, F.; Nisnevitch, M. Antibacterial Properties of Rose Bengal Immobilized in Polymer Supports. *Appl. Mech. Mater.* **2015**, *719–720*, 21–24. [[CrossRef](#)]
29. Nakonechny, F.; Nisnevitch, M.; Nitzan, Y.; Nisnevitch, M. Sonodynamic Excitation of Rose Bengal for Eradication of Gram-Positive and Gram-Negative Bacteria. *Biomed Res. Int.* **2013**, *2013*, 684930. [[CrossRef](#)] [[PubMed](#)]
30. Valkov, A.; Nakonechny, F.; Nisnevitch, M. Polymer-Immobilized Photosensitizers for Continuous Eradication of Bacteria. *Int. J. Mol. Sci.* **2014**, *15*, 14984–14996. [[CrossRef](#)] [[PubMed](#)]
31. Gurianov, Y.; Meistelman, M.; Albo, Y.; Nisnevitch, M.; Nakonechny, F. Antibacterial Activity of Rose Bengal Entrapped in Organically Modified Silica Matrices. *Int. J. Mol. Sci.* **2022**, *23*, 3716. [[CrossRef](#)] [[PubMed](#)]
32. Alarcon, E.I.; Poblete, H.; Roh, H.G.; Couture, J.F.; Comer, J.; Kochevar, I.E. Rose Bengal Binding to Collagen and Tissue Photobonding. *ACS Omega* **2017**, *2*, 6646–6657. [[CrossRef](#)] [[PubMed](#)]
33. Shrestha, A.; Hamblin, M.R.; Kishen, A. Characterization of a Conjugate between Rose Bengal and Chitosan for Targeted Antibiofilm and Tissue Stabilization Effects as a Potential Treatment of Infected Dentin. *Antimicrob. Agents Chemother.* **2012**, *56*, 4876–4884. [[CrossRef](#)] [[PubMed](#)]
34. Son, T.I.; Sakuragi, M.; Takahashi, S.; Obuse, S.; Kang, J.; Fujishiro, M.; Matsushita, H.; Gong, J.; Shimizu, S.; Tajima, Y.; et al. Visible Light-Induced Crosslinkable Gelatin. *Acta Biomater.* **2010**, *6*, 4005–4010. [[CrossRef](#)] [[PubMed](#)]
35. Schiraldi, C.; La, A.; De, M. Biotechnological Production and Application of Hyaluronan. *Biopolymers* **2010**, *20*, 10271. [[CrossRef](#)]
36. Milipore Sigma IR Spectrum Table & Charts. Available online: <https://www.sigmaaldrich.com/PH/en/technical-documents/technical-article/analytical-chemistry/photometry-and-reflectometry/ir-spectrum-table> (accessed on 2 January 2024).
37. Liao, L.F.; Lien, C.F.; Shieh, D.L.; Chen, F.C.; Lin, J.L. FTIR Study of Adsorption and Photochemistry of Amide on Powdered TiO<sub>2</sub>: Comparison of Benzamide with Acetamide. *Phys. Chem. Chem. Phys.* **2002**, *4*, 4584–4589. [[CrossRef](#)]
38. Mordechai, S.; Mordehai, J.; Ramesh, J.; Levi, C.; Huleihal, M.; Erukhimovitch, V.; Moser, A.; Kapelushnik, J. Application of FTIR Microspectroscopy for the Follow-up of Childhood Leukemia Chemotherapy. *Subsurf. Surf. Sens. Technol. Appl. III* **2001**, *4491*, 243–250. [[CrossRef](#)]
39. Gokulakumar, B.; Narayanaswamy, R. Fourier Transform—Infrared Spectra (FT-IR) Analysis of Root Rot Disease in Sesame (*Sesamum Indicum*). *Rom. J. Biophys.* **2008**, *18*, 217–223.
40. Osmond, G.; Boon, J.J.; Puskar, L.; Drennan, J. Metal Stearate Distributions in Modern Artists’ Oil Paints: Surface and Cross-Sectional Investigation of Reference Paint Films Using Conventional and Synchrotron Infrared Microspectroscopy. *Appl. Spectrosc.* **2012**, *66*, 1136–1144. [[CrossRef](#)]
41. Ryu, S.R.; Noda, I.; Jung, Y.M. What Is the Origin of Positional Fluctuation of Spectral Features: True Frequency Shift or Relative Intensity Changes of Two Overlapped Bands? *Appl. Spectrosc.* **2010**, *64*, 1017–1021. [[CrossRef](#)]
42. Ryu, S.R.; Noda, I.; Jung, Y.M. Positional Fluctuation of IR Absorption Peaks: Frequency Shift of a Single Band or Relative Intensity Changes of Overlapped Bands? *Am. Lab.* **2011**, *43*, 40–43.

43. Adre, E.; Durkee, H.; Arboleda, A.; Alawa, K.; Maestre, J.; Mintz, K.J.; Leblanc, R.M.; Amescua, G.; Parel, J.M.; Miller, D. Rose Bengal and Riboflavin Mediated Photodynamic Antimicrobial Therapy Against Selected South Florida Nocardia Keratitis Isolates. *Transl. Vis. Sci. Technol.* **2022**, *11*, 6–12. [[CrossRef](#)]
44. Fujii, M.; Usui, M.; Hayashi, S.; Gross, E.; Kovalev, D.; Künzner, N.; Diener, J.; Timoshenko, V.Y. Chemical Reaction Mediated by Excited States of Si Nanocrystals—Singlet Oxygen Formation in Solution. *J. Appl. Phys.* **2004**, *95*, 3689–3693. [[CrossRef](#)]
45. Żamojć, K.; Zdrowowicz, M.; Rudnicki-Velasquez, P.B.; Krzymiński, K.; Zaborowski, B.; Niedziałkowski, P.; Jacewicz, D.; Chmurzyński, L. The Development of 1,3-Diphenylisobenzofuran as a Highly Selective Probe for the Detection and Quantitative Determination of Hydrogen Peroxide. *Free Radic. Res.* **2017**, *51*, 38–46. [[CrossRef](#)] [[PubMed](#)]
46. Carloni, P.; Damiani, E.; Greci, L.; Stipa, P.; Tanfani, F.; Tartaglino, E.; Wozniak, M. On the Use of 1,3-Diphenylisobenzofuran (DPBF). Reactions with Carbon and Oxygen Centered Radicals in Model and Natural Systems. *Res. Chem. Intermed.* **1993**, *19*, 395–405. [[CrossRef](#)]
47. Nardello, V.; Brault, D.; Chavalle, P.; Aubry, J.M. Measurement of Photogenerated Singlet Oxygen ( $^1O_2$  ( $1\Delta(g)$ )) in Aqueous Solution by Specific Chemical Trapping with Sodium 1,3-Cyclohexadiene-1,4-Diethanoate. *J. Photochem. Photobiol. B Biol.* **1997**, *39*, 146–155. [[CrossRef](#)]
48. Harada, N.; Kataoka, M.; Nakanosho, M.; Uyama, H. Penetration of Singlet Oxygen into Films with Oxygen Permeability Coefficient Close to That of Skin. *Photochem. Photobiol.* **2021**, *97*, 971–979. [[CrossRef](#)] [[PubMed](#)]
49. Hao, Y.; Liu, B.M.; Bennett, T.F.; Monsour, C.G.; Selke, M.; Liu, Y. Determination of Singlet Oxygen Quantum Yield of a Porphyrinic Metal-Organic Framework. *J. Phys. Chem. C* **2021**, *125*, 7392–7400. [[CrossRef](#)]
50. Cantelli, A.; Piro, F.; Pecchini, P.; Di Giosia, M.; Danielli, A.; Calvaresi, M. Concanavalin A-Rose Bengal Bioconjugate for Targeted Gram-Negative Antimicrobial Photodynamic Therapy. *J. Photochem. Photobiol. B Biol.* **2020**, *206*, 111852. [[CrossRef](#)]
51. Wilkinson, F.; Helman, W.P.; Ross, A.B. Quantum Yields for the Photosensitized Formation of the Lowest Electronically Excited Singlet State of Molecular Oxygen in Solution. *J. Phys. Chem. Ref. Data* **1993**, *22*, 113–262. [[CrossRef](#)]
52. Fadel, M.; Kassab, K. Evaluation of the Photostability and Photodynamic Efficacy of Rose Bengal Loaded in Multivesicular Liposomes. *Trop. J. Pharm. Res.* **2011**, *10*, 289–297. [[CrossRef](#)]
53. Zhang, Y.; Neal, S.L. Reaction Monitoring of Rose Bengal Photodegradation in Alcohols Using Multivariate Frequency-Domain Dynamic Fluorescence. *J. Photochem. Photobiol. A Chem.* **2023**, *436*, 114348. [[CrossRef](#)]
54. Rytwo, G.; Zelkind, A.L. Evaluation of Kinetic Pseudo-Order in the Photocatalytic Degradation of Ofloxacin. *Catalysts* **2022**, *12*, 24. [[CrossRef](#)]
55. Pierański, M.K.; Kosiński, J.G.; Szymczak, K.; Sadowski, P.; Grinholc, M. Antimicrobial Photodynamic Inactivation: An Alternative for Group B Streptococcus Vaginal Colonization in a Murine Experimental Model. *Antioxidants* **2023**, *12*, 847. [[CrossRef](#)]
56. Nakonechny, F.; Barel, M.; David, A.; Koretz, S.; Litvak, B.; Ragozin, E.; Etinger, A.; Livne, O.; Pinhasi, Y.; Gellerman, G.; et al. Dark Antibacterial Activity of Rose Bengal. *Int. J. Mol. Sci.* **2019**, *20*, 3196. [[CrossRef](#)]
57. Sugita, N.; Iwase, Y.; Yumita, N.; Ikeda, T.; Umemura, S.I. Sonodynamically Induced Cell Damage Using Rose Bengal Derivative. *Anticancer Res.* **2010**, *30*, 3361–3366.
58. Štacková, L.; Muchová, E.; Russo, M.; Slavíček, P.; Štacko, P.; Klán, P. Deciphering the structure-property relations in substituted heptamethine cyanines. *J. Org. Chem.* **2020**, *85*, 9776–9790. [[CrossRef](#)]

**Disclaimer/Publisher’s Note:** The statements, opinions and data contained in all publications are solely those of the individual author(s) and contributor(s) and not of MDPI and/or the editor(s). MDPI and/or the editor(s) disclaim responsibility for any injury to people or property resulting from any ideas, methods, instructions or products referred to in the content.